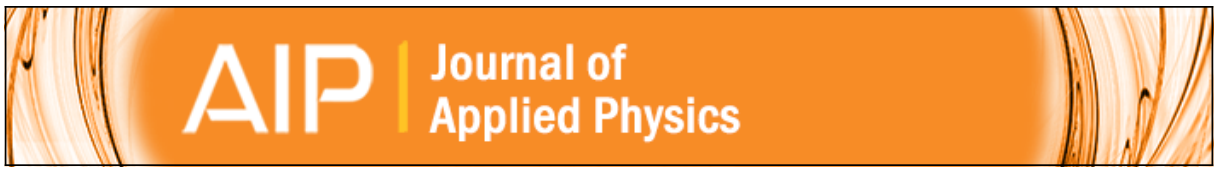

Ferromagnetic resonance of patterned chromium dioxide thin films grown by selective area chemical vapour deposition

C. J. Durrant, M. Jokubaitis, W. Yu, H. Mohamad, L. R. Shelford, P. S. Keatley, Gang Xiao, and R. J. Hicken

Citation: Journal of Applied Physics **117**, 17B707 (2015); doi: 10.1063/1.4907766

View online: http://dx.doi.org/10.1063/1.4907766

View Table of Contents: http://scitation.aip.org/content/aip/journal/jap/117/17?ver=pdfcov

Published by the AIP Publishing

Ferromagnetic resonance of patterned chromium dioxide thin films grown by selective area chemical vapour deposition

C. J. Durrant,[1,a)] M. Jokubaitis,[2] W. Yu,[1] H. Mohamad,[1] L. R. Shelford,[1] P. S. Keatley,[1] Gang Xiao,[2] and R. J. Hicken[1]
[1]*Department of Physics and Astronomy, University of Exeter, Exeter EX4 4QL, United Kingdom*
[2]*Department of Physics, Brown University, Providence, Rhode Island 02912, USA*

(Presented 5 November 2014; received 22 September 2014; accepted 20 October 2014; published online 9 February 2015)

A selective area chemical vapour deposition technique has been used to fabricate continuous and patterned epitaxial CrO_2 thin films on (100)-oriented TiO_2 substrates. Precessional magnetization dynamics were stimulated both electrically and optically, and probed by means of time-resolved Kerr microscopy and vector network analyser ferromagnetic resonance techniques. The dependence of the precession frequency and the effective damping parameter upon the static applied magnetic field were investigated. All films exhibited a large in-plane uniaxial anisotropy. The effective damping parameter was found to exhibit strong field dependence in the vicinity of the hard axis saturation field. However, continuous and patterned films were found to possess generally similar dynamic properties, confirming the suitability of the deposition technique for fabrication of future spintronic devices. © *2015 AIP Publishing LLC*. [http://dx.doi.org/10.1063/1.4907766]

Chromium dioxide (CrO_2) is a highly attractive material for spintronic applications[1,2] due to its near 100% spin polarization.[3] The realisation of CrO_2 based spintronic devises requires both the fabrication of high quality elements on a sub-micron scale, and a comprehensive understanding of their dynamical properties. Fabrication of patterned CrO_2 structures is however a complex task since CrO_2 readily decomposes to Cr_2O_3 when traditional postdeposition patterning processes, such as argon-ion milling,[4] wet etching, reactive ion etching (RIE),[5] and focused ion beam milling[6] are used. Selective-area chemical vapour deposition (CVD) of epitaxial CrO_2 onto rutile TiO_2 substrates through prepatterned amorphous SiO_2 stencils provides a promising alternative, but the dynamic properties of such structures have yet to be confirmed

Previous studies of CrO_2 nano-structures have explored their magnetotransport[7,8] and micromagnetic[9,10] properties. Ferromagnetic resonance (FMR) measurements[11,12] have been performed upon continuous CrO_2 films but were not extended to patterned elements. Ultrafast dynamics, including precession, have been measured in all-optical pump-probe setups[13,14] but with the additional complication that optical heating fundamentally alters the magnetic properties of the sample. In particular, epitaxial $CrO_2/TiO_2(100)$ films possess a large uniaxial anisotropy, with an in-plane easy axis, that has a strong temperature and thickness dependence.[15]

In the present study, Au coplanar striplines (CPS) were deposited around CrO_2 elements, grown by selective area CVD, to facilitate high frequency measurements by vector network analyser FMR (VNA-FMR) and time resolved scanning Kerr microscopy (TRSKM). Such measurements are challenging due to the large anisotropic dielectric constant of the rutile TiO_2 substrate,[16,17] and the small precession amplitude resulting from the strong uniaxial magnetic anisotropy. We explore the dynamical response observed by different measurement techniques and compare the dynamical properties of continuous and patterned films to confirm the efficacy of the selected area CVD technique.

Patterned CrO_2 films were grown in a traditional two-zone CVD[15] furnace on $5 \times 5 \times 0.5$ mm (100)-oriented single crystal rutile TiO_2 substrates[17] through a 50 nm thick SiO_2 stencil layer. The stencil was formed by sputter deposition of SiO_2 followed by a combination of photolithography and reactive ion etching. The substrate plus stencil were then cleaned and baked at 185 °C for 30 min before CVD of CrO_2. The purity of the CrO_2 phase was confirmed by X-ray diffraction (XRD) with no observable decomposition into Cr_2O_3. A Ti/Au(100 nm) CPS was then deposited around the rectangular CrO_2 elements through a further stage of photolithographic processing.

Continuous films were fabricated with thicknesses in the range of $T = 27$–1200 nm. Two patterned strips of 80 μm width and 2 mm length were grown for which $T = 55$ and 250 nm. Strips were oriented with the long edge along the [001] axis, which is expected to be the easy axis for $t < 50$ nm.[15] The CPS track width and separation were chosen to be 21 μm and 100 μm, respectively, and were intended to achieve a characteristic impedance of 50 Ω although significant error can be expected since the dielectric constant of the TiO_2 is anisotropic and poorly characterised.

The static magnetic properties of both continuous and patterned CrO_2 films were first investigated by longitudinal magneto-optical Kerr effect (MOKE) measurements performed with a 633 nm wavelength s-polarized focused laser beam. Hysteresis loops were recorded with field applied in the [001] and [010] directions.

[a)]Author to whom correspondence should be addressed. Electronic mail: cjd216@exeter.ac.uk.

VNA-FMR measurements were made on continuous films by placing the samples face down on a 50 Ω coplanar waveguide (CPW) with 500 μm signal track width. An ~ 100 nm layer of photoresist was used to prevent the sample short circuiting the CPW. The scattering matrix parameters of the composite structure were recorded as the field was swept between 0 and 1.3 kOe. VNA-FMR measurements were also attempted upon the patterned elements using wire bonding to connect to the CPS, but no measurable response was observed, presumably due to poor impedance matching and the small amplitude of precession.

Instead, TRSKM measurements were performed on the patterned samples using the setup described in Ref. 18. The CPS was connected to a 50 Ω CPW by wire bonds and the sample magnetization excited by the magnetic field associated with 6 V, 70 ps FWHM pulses supplied to the CPS. Time resolved polar MOKE measurements were made at 80 MHz repetition rate with laser pulses of 800 nm wavelength and 100 fs duration. A static field of 0–0.9 kOe was applied parallel to the [010] hard axis. No measurable signal was observed when the field was applied parallel to the easy axis, due to the higher frequency and lower amplitude of precession.

Finally, all-optical pump-probe measurements were made on selected continuous films using the setup described in Ref. 19. Optical pumping was performed with *s*-polarized pulses of 50 fs duration, 800 nm wavelength, and 2.26 mJ/cm^2 fluence at near normal incidence. Time resolved Kerr rotation measurements were made with an *s*-polarized 800 nm wavelength probe pulse incident at 45°. Pump and probe beams were focused onto the sample surface with spot sizes of 135 μm and 40 μm, respectively. Again a measurable precession response was only observed when a static field of 0.22–1.8 kOe was applied in the [010] direction.

The oscillatory part of the Kerr rotation signals were fitted to the form

$$\theta_K \propto \theta_0 \cos\left[2\pi f_0 t + \varphi\right] \exp\left(-t/\tau\right), \tag{1}$$

where θ_0, f_0, $1/\tau$, and φ are, respectively, the amplitude of precession, the frequency, the relaxation rate, and the initial phase of the precessional signal. In the all-optical and TRSKM experiments, intense optical and electrical pulses, respectively, are used to perturb the magnetic state on time scales short compared to the period of precession. After excitation, the magnetization is no longer parallel to $\mathbf{H}_{eff}$, the total effective field acting on the magnetization and a damped precession ensues. If material parameters modified by the excitation relax sufficiently slowly compared to its period, the precession may be described by the Landau-Lifshitz-Gilbert equation

$$\frac{\partial \mathbf{M}}{\partial t} = -|\gamma|\mathbf{M} \times \mathbf{H}_{eff} + \frac{\alpha}{\mathrm{M}}\left(\mathbf{M} \times \frac{\partial \mathbf{M}}{\partial t}\right), \tag{2}$$

where α is the phenomenological damping parameter, $\gamma = 2.8 \times \pi \times g\,\mathrm{MHz/Oe}$ is the gyromagnetic ratio of the electron, and g is the spectroscopic splitting factor. In the limit $\alpha \ll 1$, the apparent damping parameter α, which contains contributions from all damping processes present, is given by[19]

$$\alpha = \frac{2}{|\gamma|(H_\alpha + H_\beta)}\frac{1}{\tau}, \tag{3}$$

where H_α and H_β are effective fields that include the anisotropy and demagnetizing fields.[19] For a frequency domain measurement such as VNA-FMR, the relaxation rate $1/\tau$ is replaced by the half width at half maximum frequency $\Delta\omega_{FWHM}/2$.

Typical MOKE hysteresis loops with **H** applied in the [010] and [001] directions, for both patterned and continuous films, are shown in Figure 1. All samples show strong uniaxial anisotropy with a [001] easy axis. A difference in loop height is observed for the easy and hard axis due to the birefringent nature of the film and substrate. Hard axis loops for patterned samples (Figures 1(b) and 1(c)) deviate from the expected linear shape, probably due to slight misalignment of **H** from the hard axis and mixing of first and second order Kerr effects. The hard axis saturation field, $H_k = 2K_u/M_S$, where K_u is the uniaxial anisotropy constant and M_s is the saturation magnetization, was extracted from the loops and used in the fitting of dynamic results. This anisotropy field increases with film thickness as previously reported.[11,12]

The results of VNA-FMR measurements performed on a 250 nm continuous film are presented in Figure 2. The effect of the uniaxial in plane anisotropy is immediately apparent from panels (a) and (e). With **H** applied along the [001] (easy) axis, the FMR frequency increases monotonically with **H**, while for the [010] axis a minimum is observed as **H** approaches the hard axis saturation field. Cross-sections through the grey scale plot may be taken as a function of field, as in the lower panels, or frequency. In the latter case, the absorptive (imaginary) component of the scattering

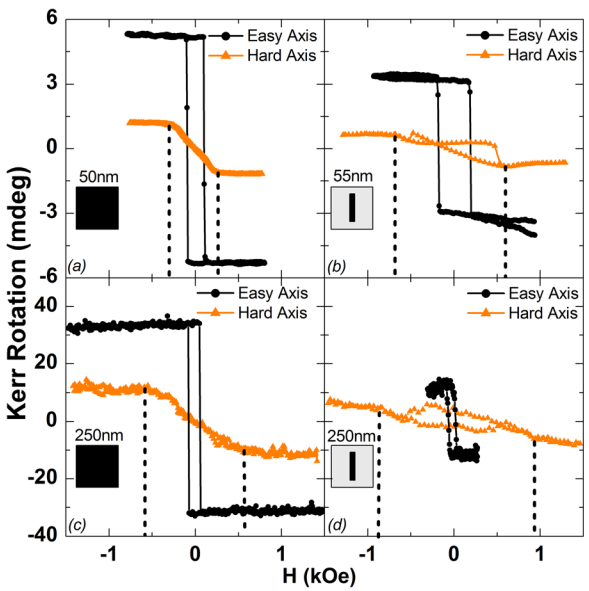

FIG. 1. MOKE loops with field along the easy [001] and hard [010] axes for (a) T = 50 nm continuous; (b) T = 55 nm, 80 μm wide strip; (c) T = 250 nm continuous; and (d) T = 250 nm, 80 μm wide strip, CrO_2 samples. Dashed lines indicate H_k in each case.

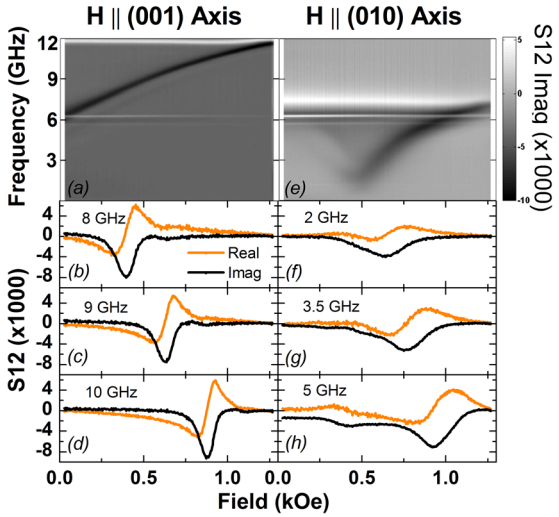

FIG. 2. VNA-FMR measurement of 250 nm continuous film, with H parallel to (001) in (a)–(d) and (010) in (e)–(h). (a) and (e) $Im(S_{12})$ while both $Re(S_{12})$ and $Im(S_{12})$ are plotted against field for selected frequencies in the remaining panels.

matrix representing transmitted power S_{12} was fitted to a Lorentzian function, and the linewidth used to calculate α.

Since attempts to measure the patterned elements by VNA-FMR proved unsuccessful, TRSKM was used to perform time domain measurements on samples with $T = 55$ and 250 nm. The time resolved polar MOKE response of a $T = 55$ nm strip is displayed in Figure 3(a). **H** was again applied parallel to the [010] axis and H varied from 0 to 0.9 kOe. The shape of the first anti-node is generally rather unclear. Measurements of the transmitted and reflected electrical pulse confirmed the presence of secondary pulses of lower amplitude resulting from poor impedance matching between the CPW and CPS structures. This can lead to a

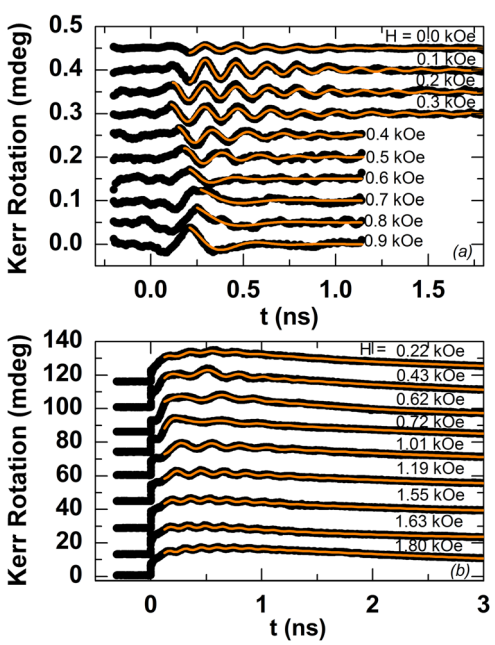

FIG. 3. (a) TRSKM measurements of a T = 55 nm, 80 μm wide CrO_2 strip. Fitted curves are shown in orange. (b) All-optical measurements of a T = 250 nm continuous CrO_2 film.

partial coherent suppression/enhancement of the precession. However, these effects appear to be confined to the first few hundred ps of the measurement, and so, fitting to Eq. (1) was performed from the first clear peak in the signal.

Finally, all-optical measurements were performed on a $T = 250$ nm continuous film for comparison. The transient polar Kerr rotation is plotted in Figure 3(b) for the field applied along the [010] hard axis. A partial ultrafast demagnetisation occurs within the first few ps, after which the uniaxial anisotropy field is reduced, initiating precession of the magnetization. The maximum Kerr signal occurs after ~300 ps, reflecting a slower demagnetization process associated with the half metallic character of the CrO_2.[14] Following the measurement, the data were fitted to the sum of Eq. (1) and a slowly varying background term. In addition, a term bt^2 was added to the argument of the cosine function to account for chirp that occurs as the values of magnetic parameters such as M_s and K_u gradually relax.

The precession frequencies and effective damping parameters obtained from the 3 dynamical measurement techniques are compared in Figure 4. The same characteristic field dependence of the frequency is observed in all cases when the field is applied parallel to the hard axis. Indeed, the optical experiments only yielded measurable signals in this configuration since the frequency is lower and the amplitude of precession greater. The VNA-FMR measurements show that α is only weakly field dependent when **H** is applied along the [001] (easy) axis but varies strongly when **H** is along the [010] (hard) axis. Specifically, we observe an increase in α with decreasing precession frequency as **H** approaches H_k. Above H_k, the variation of α is consistent with the linear dependence reported by others.[13] Qualitatively similar behaviour is observed for all samples although the size of the uniaxial anisotropy and damping differs most significantly between the $T = 50$ and 55 nm samples, perhaps reflecting a sensitivity to substrate conditions.

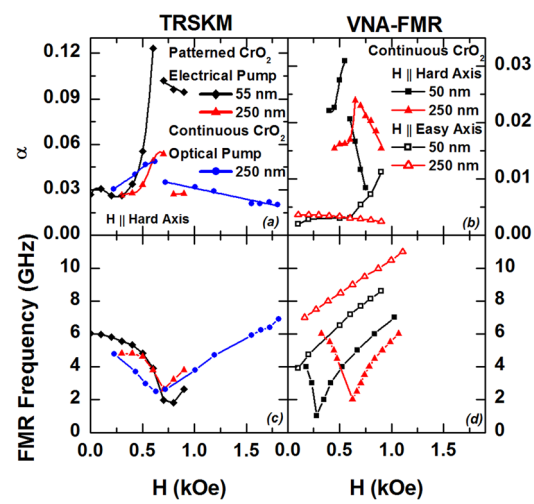

FIG. 4. Field dependence of the effective damping parameter α measured for continuous and patterned films in 3 separate experimental geometries (a) electrically and optically pumped TRSKM (b) VNA-FMR. The field dependence of the precessional frequency (c) electrically and optically pumped TRSKM (d) VNA-FMR. Lines are guides to the eye.

In summary, the large uniaxial in plane anisotropy observed in continuous and patterned epitaxial CrO_2 thin films, and the dielectric properties of their TiO_2 substrates, makes characterization of their dynamic properties challenging. Nevertheless, by comparing results obtained from complementary dynamical measurement techniques, it has been shown that continuous and patterned CrO_2 samples exhibit essentially similar dynamic magnetic properties. This bodes well for the use of CrO_2 in spintronic devices if the large anisotropy field can be accommodated.

[1]W. E. Pickett and J. S. Moodera, Phys. Today **54**(5), 39 (2001).
[2]G. Ju, A. Vertikov, A. V. Nurmikko, C. Canady, G. Xiao, R. F. C. Farrow, and A. Cebollada, Phys. Rev. B **57**, R700 (1998).
[3]Y. Ji, G. J. Strijkers, F. Y. Yang, C. L. Chien, J. M. Byers, A. Anguelouch, G. Xiao, and A. Gupta, Phys. Rev. Lett. **86**, 5585 (2001).
[4]C. Konig, M. Fonin, M. Laufenberg, A. Biehler, W. Buhrer, M. Klaui, U. Rudiger, and G. Guntherodt, Phys. Rev. B **75**, 144428 (2007).
[5]Q. Zhang, Y. Li, A. V. Nurmikko, G. X. Miao, G. Xiao, and A. Gupta, J. Appl. Phys. **96**, 7527 (2004).
[6]L. Yuan, Y. Ovchenkov, A. Sokolov, C.-S. Yang, B. Doubin, and S. H. Liou, J. Appl. Phys. **93**, 6850 (2003).
[7]X. Zou and G. Xiao, Phys. Rev. B **77**, 054417 (2008).
[8]X. Zou, G. Xiao, S. Huang, T. Chen, and C. L. Chien, J. Appl. Phys. **103**, 07D710 (2008).
[9]X. Zou and G. Xiao, Appl. Phys. Lett. **91**, 113512 (2007).
[10]X. Zou and G. Xiao, J. Appl. Phys. **103**, 07D701 (2008).
[11]B. Z. Rameev, A. Gupta, G. X. Miao, G. Xiao, F. Yildiz, L. R. Tagirov, and B. Aktaş, Phys. Status Solidi A **201**(15), 3350–3353 (2004).
[12]B. Z. Rameev, A. Gupta, G. Miao, G. Xiao, F. Yildiz, L. R. Tagirov, and B. Akta, Tech. Phys. Lett. **31**(9), 802–805 (2005).
[13]G. M. Müller, M. Münzenberg, G.-X. Miao, and A. Gupta, Phys. Rev. B. **77**, 020412 (2008).
[14]Q. Zhang, A. V. Nurmikko, G.-X. Miao, G. Xiao, and A. Gupta, Phys. Rev. B. **74**, 064414 (2006).
[15]G.-X. Miao, G. Xiao, and A. Gupta, Phys. Rev. B. **71**, 094418 (2005).
[16]R. A. Parker, Phys. Rev. **124**, 1719 (1961).
[17]See http://www.crystec.de/daten/tio2.pdf for Crystec, TiO2 datasheet (2014).
[18]P. S. Keatley, V. V. Kruglyak, R. J. Hicken, J. R. Childress, and J. A. Katine, J. Magn. Magn. Mater. **306**, 298 (2006).
[19]Y. Liu, L. R. Shelford, V. V. Kruglyak, R. J. Hicken, Y. Sakuraba, M. Oogane, Y. Ando, and T. Miyazaki, J. Appl. Phys. **101**, 09C106 (2007).